

# NUMERICAL ANALYSIS OF HUB AND FUSELAGE INTERFERENCE TO REDUCE HELICOPTER DRAG

Walid Khier, walid.khier@dlr.de, DLR, Braunschweig, Germany

## Abstract

A numerical investigation was carried out to predict the mutual interference between helicopter components. The investigation was based on the solution of RANS equations in three dimensions using unstructured grids. Results are presented for six different test cases under steady forward flight conditions at Mach number equal to 0.204. These test cases refer to different combinations of reduced scale models of helicopter fuselage, rotor hub and main rotor modelled by an actuator disc. Analysis of the results revealed that while significant correlation between the hub and fuselage loads, and a non trivial influence of the actuator disc on these loads could be observed, the drag breakdown of the hub was not effectively altered.

## 1. INTRODUCTION

Present day environmental regulations place severe constraints on helicopter exhaust emissions, with expectations of more restrictive future regulations for helicopter efficiency and fuel consumption. The European Commission 7th Framework Programme for collaborative research has defined therefore the reduction of helicopter aerodynamic drag as one of the main goals of its "Clean Sky" Joint Technology Initiative (JTI). For this purpose, a separate dedicated platform was established within JTI under the name Green Rotorcraft (GRC).

Helicopter main rotor hubs are known as a major source of drag. Roughly 25-30% of the drag of a single main rotor helicopter is attributed to the hub. At the same time, little has been done since the evolution of helicopters to enhance their aerodynamic characteristics. Therefore, a significant potential exists to reduce the overall drag of the helicopter by improving the performance of the hub.

Earlier investigations ([5]-[12]) indicated an important role of aerodynamic interference to drag generation. The hub and the rotor alter the flow around the fuselage affecting thereby its drag and vice versa. Proper analysis of interference mechanisms between the fuselage, hub, and possibly the rotor is therefore a prerequisite for any drag reduction attempt to be successful. Computational Fluid Dynamics is a powerful tool to assess these interference effects. It also provides a detailed insight of the flow field assisting thereby to establish a correlation between aerodynamic loads and the flow physics. The prediction of rotor hub

drag by CFD remains a challenge due to the geometrical complexity and massive interaction between rotating and non-rotating parts of a helicopter. Several published CFD investigations of rotor hub aerodynamics [13]-[15] could demonstrate, however, that present day CFD tools are capable to analyze this class of flow problems reliably.

This paper reports results of hub drag reduction investigations performed by DLR within the GRC programme. A number of three-dimensional RANS simulations of isolated components and different combinations thereof are presented. The resulting aerodynamic loads and surface pressure data are analyzed to assess the aerodynamic interference.

The purpose of the investigation is three folds: 1) to gain better understanding of the aerodynamic interference between helicopter components by comparing the aerodynamic loads acting on different configurations and their individual components. 2) To define a computational configuration to be used in rotor hub optimization. 3) And to guide planned wind tunnel experiments aimed at main rotor hub drag reduction.

## 2. THE GRC2 COMMON PLATFORM HELICOPTER MODEL

The GRC2 Common platform helicopter model was derived from the 1:3.881th scale GOAHEAD ([1] and [2]) wind tunnel model (Figure 1). All of the major components of a typical rotor head were simplified by removing tiny details, like wires, connectors,...etc. and by reducing the shapes of the components to simple geometry as indicated in Figure 2. Detailed description of the original model

and the geometrical modifications introduced are given in [3]

### 3. NUMERICAL APPROACH

#### 3.1. Description of the solver

The numerical approach employed in this paper is based on the solution of the stationary Reynolds (Favre) averaged Navier-Stokes equations in three dimensions by means of the DLR CFD simulation code TAU [4]. The solver relies on an edge-based dual-cell approach, (i.e. a cell vertex) scheme to discretize the mass, momentum and energy fluxes, which are represented by either central scheme or a variety of upwind schemes (for the inviscid fluxes) using linear reconstruction of the left and right states to ensure second-order accuracy. Third order numerical dissipation is added to the convective fluxes to ensure numerical stability. The dissipative fluxes are computed using either scalar or matrix formulation. The solver also features Low Mach number preconditioning to extend the application of the code to the incompressible regimes. Multi-stage Runge-Kutta explicit as well as implicit LU-SGS (not employed in this paper) time integration schemes are used to advance the solution in artificial time in the case of steady simulation, and dual-time approach is employed for time accurate simulations. TAU allows rotors and propellers to be presented by an actuator disc following the original Froude actuator disc model but with modifications to handle compressibility effects. Chimera technique [16]-[18] is available to facilitate grid generation task and to perform simulations involving relative body motion. Turbulence effects are simulated statistically. A wide array of turbulence models, ranging from algebraic and one-equation eddy viscosity models [19]-[21] to seven-equation Reynolds stress model ([22]-[24]).

#### 3.2. Selection and Definition of Test Cases

To assess the mutual interaction between the rotor hub and the fuselage, six different configurations were considered (see Figure 3)

1. TC1: Isolated complete rotor hub
2. TC2: Configuration TC1 without push rods
3. TC3: Configuration TC2 + fuselage
4. TC4: Configuration TC3 + Actuator disc
5. TC5: Configuration TC2 without rotor hub (Isolated fuselage)
6. TC6: Configuration TC4 without rotor hub (fuselage + Actuator disc)

Push rods effect on the resulting forces is negligible owing to their tiny geometrical dimensions and to being largely protected from the oncoming flow by the shaft fairing. Their inclusion seems not to justify the associated computational overhead. Therefore, configuration TC2 was defined to verify their influence on the hub forces. Configuration TC3 is intended to study the effects of the rotor hub on the fuselage and vice versa, by comparison with configuration TC5, while configuration TC4 should show how the rotor downwash affects the results of configuration TC3. The mutual influence of the rotor hub and fuselage is examined with and without the presence of the rotor by comparing both configurations TC6 with TC4, and configurations TC3 with TC5.

#### 3.3. Numerical Parameters and Flight Conditions

All the test cases refer to steady forward flight cruise and zero pitch ( $\alpha=0^\circ$ ) and zero side slip ( $\beta=0^\circ$ ) conditions at Mach number  $M=0.2$ . Isolated rotor hub configurations were tested under two fuselage angles of attack,  $\alpha=0^\circ, 5^\circ$ . Explicit five-stage Runge-Kutta time stepping combined with five-level multi-grid was employed to advance the solution to steady state. Central scheme with artificial dissipation was used for the convective fluxes. Turbulence effects were introduced by Wilcox's two-equation  $k-\omega$  model [20]. Table 1 summarizes the flight and flow conditions for all test cases.

No slip conditions were specified for solid walls. Isolated hub cases (TC1 and TC2) were considered in free stream with far field boundary conditions applied on all external boundaries. All other cases simulate internal flow in 8 m x 6 m test section with the origin at the rotor's centre. Slip walls are defined for all tunnel walls, reservoir-pressure conditions were applied at the inflow and predefined pressure was set at the outflow boundaries.

#### 3.4. Numerical Grid

For the isolated hub cases, additional volume domains were added to the hub grid to move the free stream boundaries far enough from the hub while maintaining identical grid characteristics in the near field. Periodic hybrid grids were generated around one quarter of the hub then duplicated and merged using an in house tool to insure perfect rotational symmetry. CENTAUR® was chosen for the grid generation task because its compatibility with TAU actuator disc database.

	$M_\infty$ [-]	$\alpha$ [°]	$\beta$ [°]	$Re$ [1/m]
TC1.a	0.2	5	0	$4.6 \times 10^6$
TC1.b	0.2	0	0	$4.6 \times 10^6$
TC2.a	0.2	5	0	$4.6 \times 10^6$
TC2.b	0.2	0	0	$4.6 \times 10^6$
TC3	0.2	0	0	$4.6 \times 10^6$
TC4	0.2	0	0	$4.6 \times 10^6$
TC5	0.2	0	0	$4.6 \times 10^6$
TC6	0.2	0	0	$4.6 \times 10^6$

Table 1: Summary of flight conditions. Angle ( $\alpha$ ) values refers to the fuselage pitch altitude.

Separate grids were generated around the rotor hub and the fuselage plus actuator disc, and were later combined by Chimera to produce the different configurations mentioned earlier (Figure 4).

	Hub	Fuselage
No. of Points	20797267	3552916
No. of Tetra hydra	19775028	6512169
No. of Prisms	33865576	4528505

Table 2: Grid parameters

#### 4. RESULTS

The effect of the actuator disc on the drag breakdown of the complete configuration is shown in Figure 5 which depicts the drag breakdown for cases TC3 and TC4. Including the actuator disc reduces mainly the drag of the fuselage (as will be shown later), and has negligible influence on the drag of the hub thus leading to an increase of 5% in the share of the hub to the overall drag.

Figure 6 compares the fuselage forces for cases TC3, TC4, TC5 and TC6 normalized by the values of TC4. Examination of TC5 and TC6 indicates

negligible effects of the actuator disc on the drag of the fuselage in the absence of the rotor hub. The presence of the hub (TC3) increases the fuselage drag to more than 230% of isolated fuselage drag of TC5, but the rotor reduced it to 160% for TC4.

Different trends are observed in TC4 when the actuator disc-hub combination is considered than what is seen for individual components. Isolated fuselage (TC5) experiences almost no side force at all. The actuator disc (TC6) increases the side force considerably, and the hub (TC3) causes more dramatic increase. However, their combination brings the force down for configuration TC4 as can be shown in the figure. The rotor hub leads to an evident increase in lift in TC3 compared to the isolated fuselage TC5. The same is found for the actuator disc case, TC4 and TC6, but to a lesser extent.

Comparison of TC1 and TC2 in Figure 7 reveals negligible influence of the push rods on the drag of the hub. Removing the push rods in TC2.a and b reduces the drag by 4.3% and 4% relative to TC1.a and b, respectively. Reducing  $\alpha$  from 5° to 0° (equivalent to mast angles 0° and -5° respectively) increases the drag of the full and reduced isolated hubs (TC1 and TC2) by 5.4% and 5.7%, respectively. Although the rotor hub is partially hidden inside the fuselage in TC3 and TC4, it experiences increased dynamic pressure caused by flow acceleration over the fuselage. This leads to 25% and 20% higher drag relative to the isolated hub at zero mast inclination (TC1.a). Comparing the drag of TC3 and TC4 with TC2.b, which shares the same hub geometry and mast angle, drag increase of 23% and 18% are respectively obtained.

Higher sensitivity of the side and lift forces to the presence of the fuselage is observed than in the case of drag. While the side force falls nearly to half of its value at zero mast angle (5° fuselage pitch - TC1.a and TC2.a) by reducing the mast angle to -5° (0° fuselage pitch -TC1.b and TC2.b), interference with the fuselage causes the side force to soar reaching 450% for TC3, and 650% for TC4 of the TC1.a forces. A similar trend can be observed for the lift. Forward mast inclination in cases TC1.b and TC2.b diminishes the lift of isolated hub to 3% of its original value. These values increase two orders of magnitudes in TC3, and slightly less in TC4 due to the rotor. It must be noted however that these dramatic changes in forces are not reflection of equally dramatic variations in flow physics, rather of purely arithmetic nature caused by normalization with small lift and side force values.

Regardless of the absolute value of the drag of the hub, its breakdown given in Figure 8 shows almost the same pattern for all configurations. The major

contributors to the drag are the blade attachments with 62-73% of the drag, divided nearly 2:1 between the stubs and forks. The shaft and hub assembly comes second contributing by approximately 21-30%, while the contribution of the dampers and push rods (when included) is below 10%.

Computed surface pressure for case TC1.a and TC2.a are illustrated in Figure 9. Except for the push rods, very similar pressure patterns are found on the upper and lower side. Equivalent similarities are also observed between the isolated hub cases TC1.b and TC2.b (Figure 9). For the cases including the fuselage (TC3 and TC4), larger stagnation areas are found (Figure 10), indicating the influence of flow acceleration as pointed out earlier. Figure 11 depicts distributions of pressure differences on the hub between TC3 and TC4 indicating relative pressure and suction zones created by the rotor wake and downwash. Large pressure zone can be seen on the upper surface of the retreating stub, and hub cap, while smaller zone is generated on advancing stub, which most probably the reason of the drop in lift observed in Figure 7.

The influence of fuselage-hub-actuator disc interference on the fuselage is best indicated by the pressure difference contours presented in Figure 12 to Figure 16. Figure 12 shows clearly that the hub generally reduces surface pressure except for the top of the mast fairing, windshield, lower side of the horizontal stabilizer and the front part of the engine fairing, leading to the rise in lift observed between TC5 and TC3 in Figure 6.

Broadly the same comments can be made on Figure 13 illustrating the differences between TC4 and TC6. The rotor downwash reduces the values of lift, but does not seem to strongly alter the flow pattern around the aircraft. Figure 14 shows the effect of the rotor downwash on the fuselage by subtracting TC5 surface pressure from TC6. It can be clearly seen that the presence of the rotor causes a global pressure increase on the fuselage, except the top of the engine fairing and the lower side of the horizontal stabilizer. The integral effect of these changes in pressure is the strong drop in lift observed in Figure 6 between the isolated fuselage (TC5) and the fuselage-actuator disc configuration (TC6).

Inspection of surface pressure differences obtained by subtracting TC3 data from TC4 shows how the presence of the hub alters the behaviour of the actuator disc. The hub creates a low pressure area inside the mast fairing as shown in Figure 15. The net result is a reduction of the down force generated by the actuator disc seen in Figure 6 between TC5 and TC6. Finally, Figure 16 illustrates the differences in surface pressure between the full

configuration, TC4, and the isolated fuselage, TC5. A similar pattern to that introduced in Figure 12 is observed with pressure reduction of the rear part of the mast fairing and pressure increase on its top and on the wind shield.

## 5. CONCLUSIONS

- The presence of the fuselage increases the rotor hub drag by about 20%, but the associated increase in lift can be significantly higher.
- The contribution of push rods to the drag of isolated the rotor hub is in the order of 4%. For a complete configuration, this contribution is expected to be more trivial.
- The drag of the hub does not strongly depend on the actuator disc. The variation caused by the actuator disc was about 4%.
- The rotor hub alters the effect of the actuator disc on the fuselage forces. While the actuator disc hardly influences the drag of an isolated fuselage, the drag of the fuselage in fuselage-hub configuration falls to 73% of its value when the actuator disc is introduced.
- The drag of the fuselage increases to around 230% due to the presence of the hub.
- The hub converts the negative lift experienced by isolated fuselage and fuselage-rotor configurations to positive lift.
- Perhaps the most important finding is that all drag break down patterns of the hub obtained were similar for all configurations, and that the blade stubs are the major source of drag, while the hub cap comes in the third place behind the forks. The effect of the push rods and dampers is too trivial to justify the computational overhead necessary to include them in the optimization process.

## Acknowledgment

The author would like to acknowledge the European Union for funding the Clean Sky Project which supported this research in the Green Rotorcraft ITD (Contract Number CSJU-GAM-GRC-2008-00).

## 6. REFERENCES

- [1] Pahlke, K., The GOAHEAD project, Proceedings of the 33<sup>rd</sup> European Rotorcraft Forum, Kazan, Russia, September 2007.

- [2] Schwarz, T.; Pahlke, K., CFD code validation for complete helicopters - The European GOAHEAD project, American Helicopter Society 67th Annual Forum, Virginia Beach, VA, May 3-5, 2011
- [3] D'Alascio, A. Kneisch, T., Specification of geometrical constraints and of the design points for common helicopter platform optimisation subtasks. GRC2 document CSJU/ITD GRC/RP/2.2.2/32024 – Issue 1 (xx.07.2010)
- [4] Schwamborn, D.; Gerhold, T.; Heinrich R., The DLR Tau-code: Recent Applications In Research and Industry. In: Proceeding of ECCOMAS CFD 2006, Egmond aan Zee, Netherlands, September 5<sup>th</sup>-8<sup>th</sup>, 2006.
- [5] Sheehy, T., et al, A Method for Predicting Helicopter Hub Drag, United Technologies Corporation Report Nr. AD-A021 201, January 1976.
- [6] Sheehy, T., A General Review of Helicopter Rotor Hub Drag Data, AHS Meeting, Stratford, December 1975
- [7] Strob, R. H., Young, L. A., Graham, D. R., Louie, A. W., Investigation of Generic Hub Fairing and Pylon Shapes to Reduce Hub Drag, NASA Technical Memorandum 100008, September 1987
- [8] Graham, D. R., Sung, D. Y., Young, L. A., Louie, A. W., Stroub, R. H., Helicopter Hub Fairing and Pylon Interference Drag, NASA Technical Memorandum 101052, January 1989
- [9] Sung, D. Y., Lance, M. B., Young, L. A., Stroub, R. H., An Experimental Investigation of Rotor Hub Fairing Drag Characteristics, NASA Technical Memorandum 102182, September 1989
- [10] Young, L. A., Graham, D. R., Experimental Investigation of Rotorcraft Hub and Shaft Fairing Drag Reduction, AIAA 86-1783.
- [11] Young, L. A., Graham, D. R., Strob, R. H., Experimental Investigation of Rotorcraft Hub and Shaft Fairing Drag Reduction, Journal of Aircraft Vol. 24, Nr. 12 December 1987.
- [12] G. E. Sweet, J. L. Jenkins, Wind Tunnel Investigation of the Drag and Static Stability Characteristics of Four Helicopter Fuselage Models, NASA TN D-1363, July 1962.
- [13] Borie, S. et al., Influence of Rotor Wakes on Helicopter Aerodynamic Behaviour”, 35th European Rotorcraft Forum, Hamburg, 2009.
- [14] Bridgeman, J. O., Lancaster, G. T., Predicting Hub Drag on Realistic Geometries, American Helicopter Society Aeromechanics Specialists’ Conference, San Francisco, 2010.
- [15] Wake, B. E. et al., Assessment of helicopter hub drag prediction with an unstructured flow solver, American Helicopter Society 65th Annual Forum, Grapevine, Texas, May27-29, 200
- [16] Benek, J.A., Steger, J. L., Dougherty, F. C., A flexible grid embedding technique with application to the Euler equations. In 6th Computational Fluid Dynamics Conference, Danvers, MA. AIAA 83-1944, 1983.
- [17] Schwarz, T., An Interpolation Method Maintaining the Wall Distance for Structured and Unstructured Overset Grids, CEAS 2009 European Air and Space Conference, Manchester, UK, 26 - 29 October 2009
- [18] Madrane, A.; Raichle, A.; Stürmer, A., Parallel Implementation of a Dynamic Overset Unstructured Grid Approach. In: ECCOMAS 2004, Jyväskylä,, Finland, 24.-28. July 2004
- [19] Spalart, P. R., Allmaras, S. R., A One-Equation Turbulence Model for Aerodynamic Flows, AIAA 30th Aerospace Sciences Meeting and Exhibit., Reno, NV, USA, 6-9 January, 1992.
- [20] Wicox, D., C., Reassessment of the Scale-Determining Equations for Advanced Turbulence Models, AIAA Journal, vol. 26, no. 11, November 1988
- [21] Menter, F. R., Two-Equation Eddy-Viscosity Turbulence Models for Engineering Applications, AIAA Journal Vol. 32 No. 8, August 1994.
- [22] Launder, B. E., Reece, G. J., Rodi, W., Progress in the Development of a Reynolds-Stress Turbulence Closure, Journal of Fluid Mechanics, 68: 537-566, 1975.
- [23] Speziale, C. G., Sarkar, S., Gatski, T. B., Modelling the Pressure-Strain Correlation of Turbulence: An Invariant Dynamical Systems Approach. Journal of Fluid Mechanics, 227, 245-272, 1991.
- [24] Eisfeld, B., Brodersen, O., Advanced Turbulence Modelling and Stress Analysis for the DLR-F6 Configuration. 23rd AIAA Applied Aerodynamics Conference, 6-9 June 2005, Toronto, Canada.



Figure 1: The GOAHEAD configuration inside the DNW-LLF wind tunnel

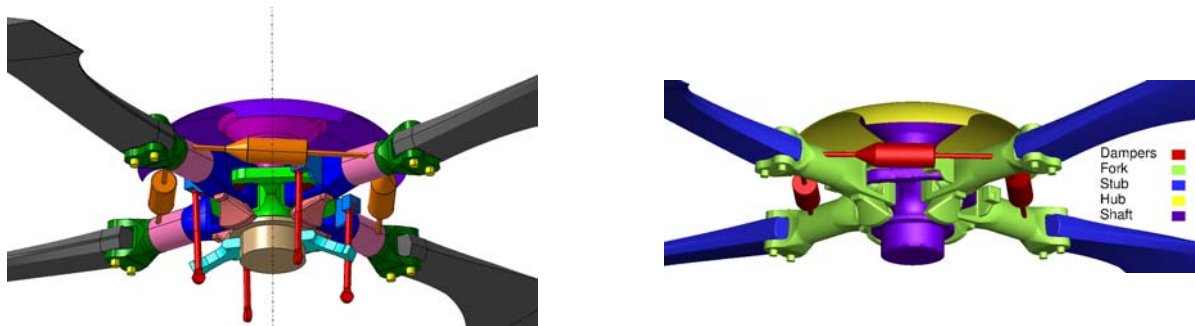
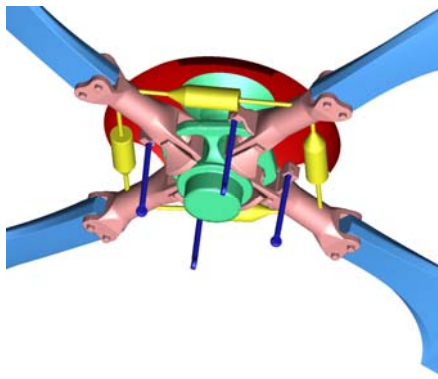
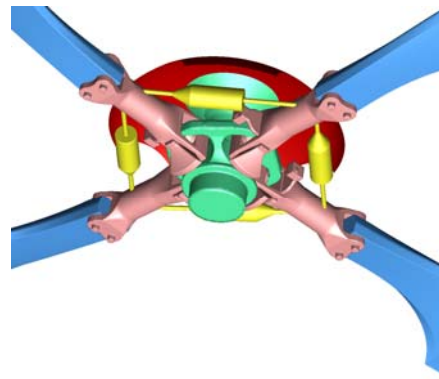


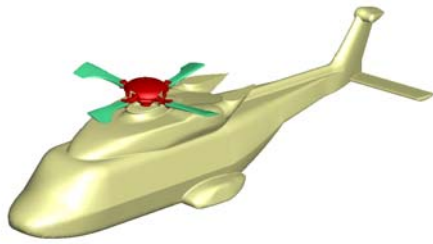
Figure 2: CAD model of the simplified common platform helicopter rotor head (left). Right: computational model of the hub showing its main components (excluding push rods)



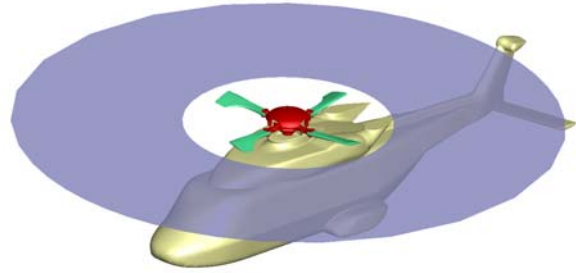
TC1



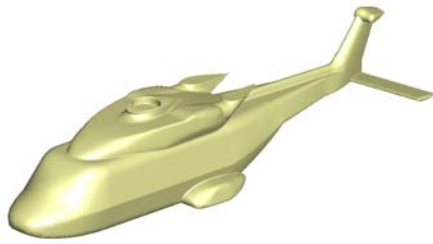
TC2



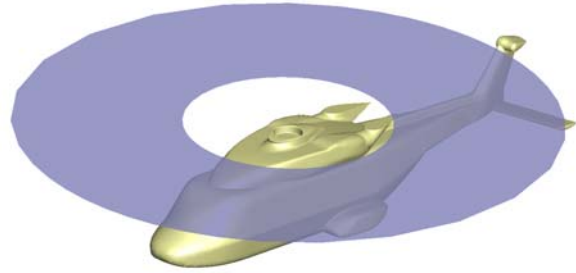
TC3



TC4



TC5



TC6

Figure 3: Definition of the computational models analysed

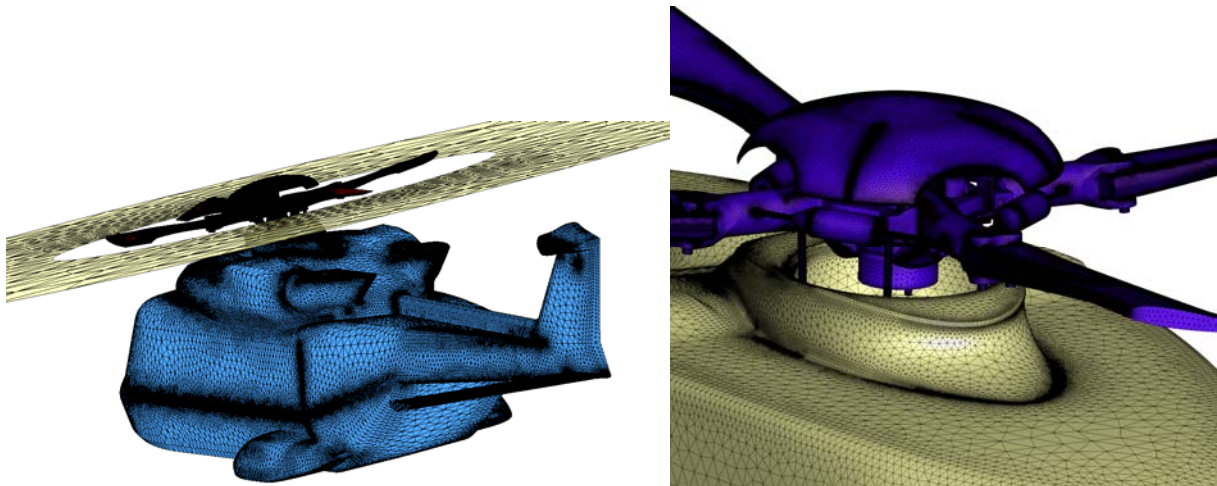


Figure 4: Surface grid on the fuselage, the actuator disc and rotor hub

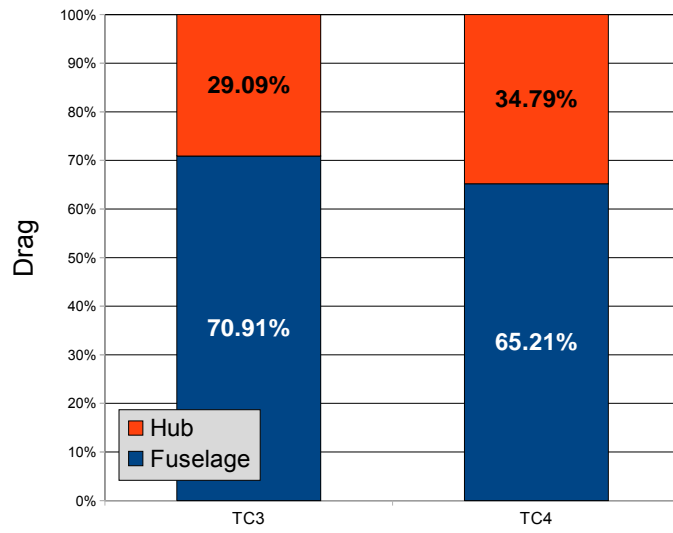


Figure 5: Drag breakdown TC3 and TC4

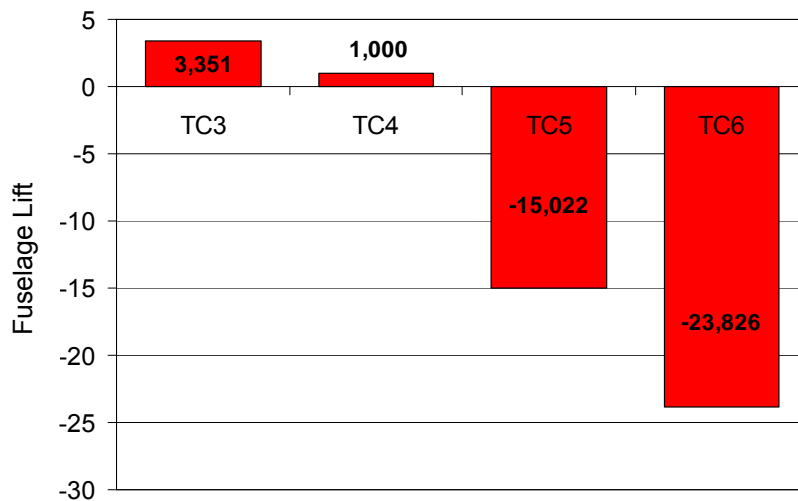
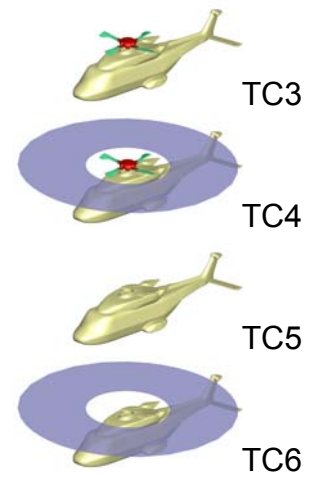
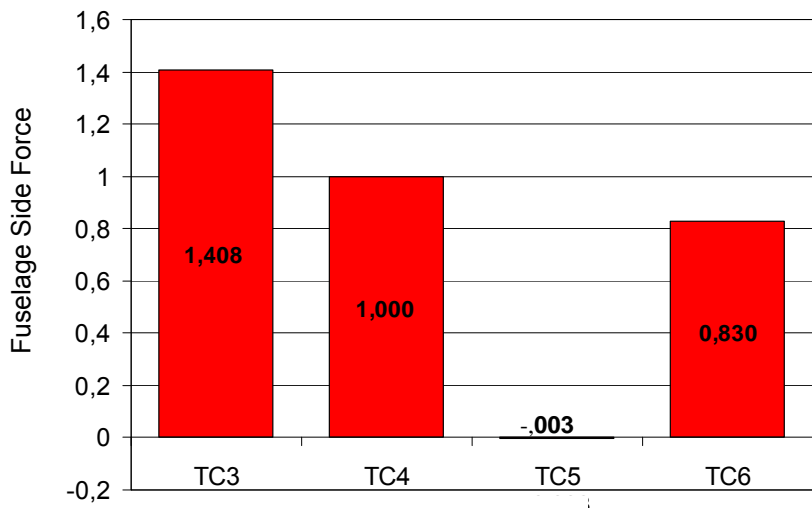
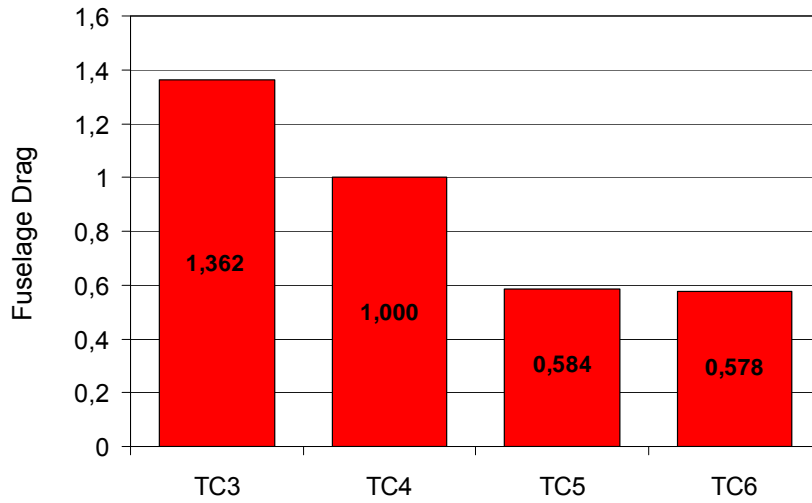


Figure 6: Fuselage drag, side force and lift coefficients for different configurations normalized by the values of TC4

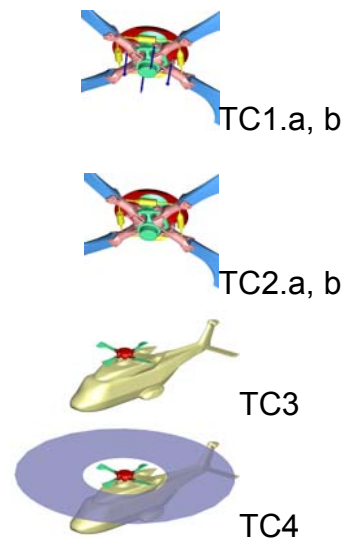
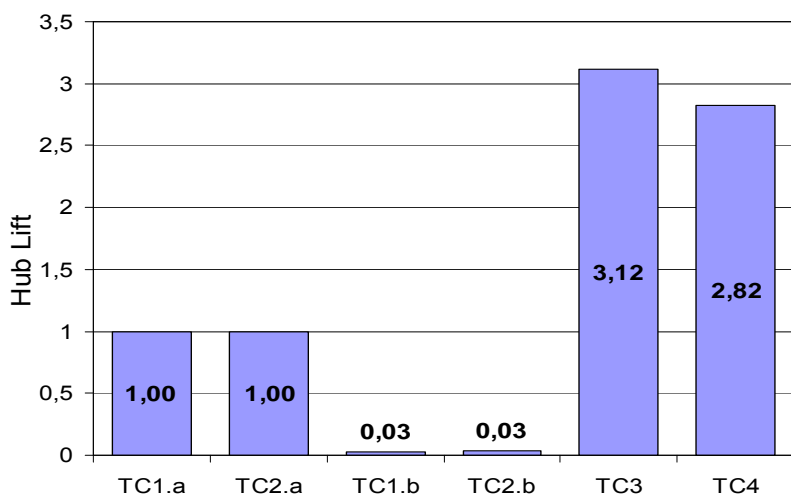
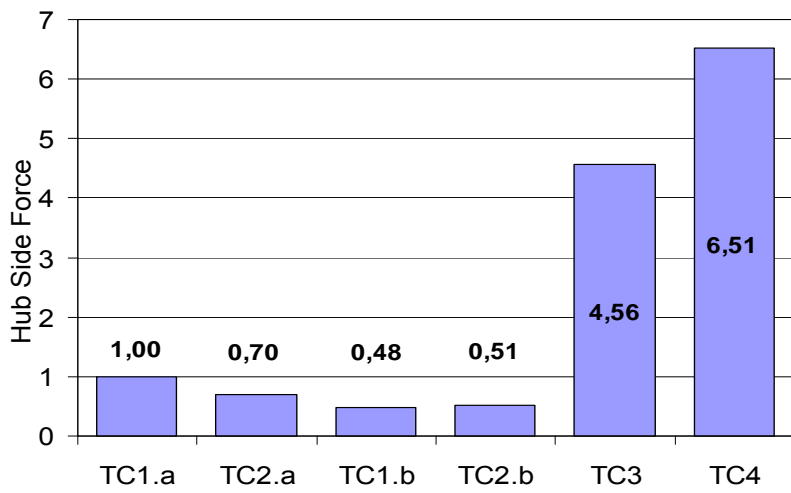
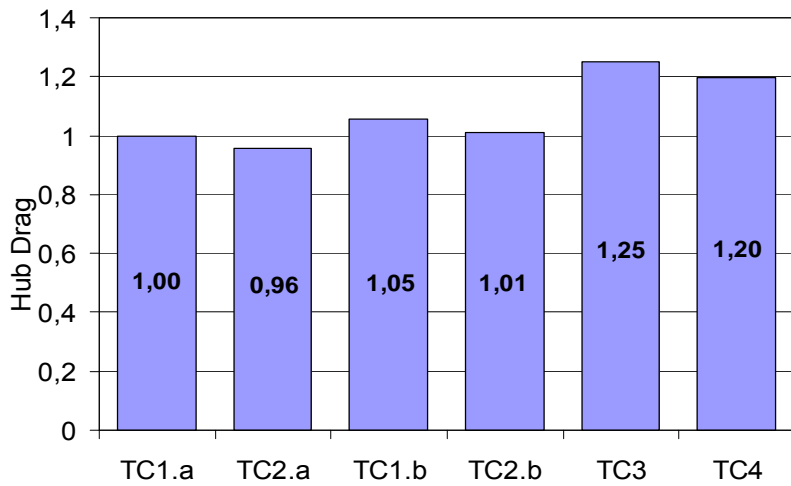
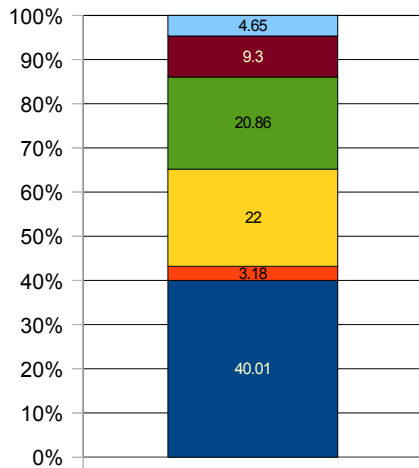
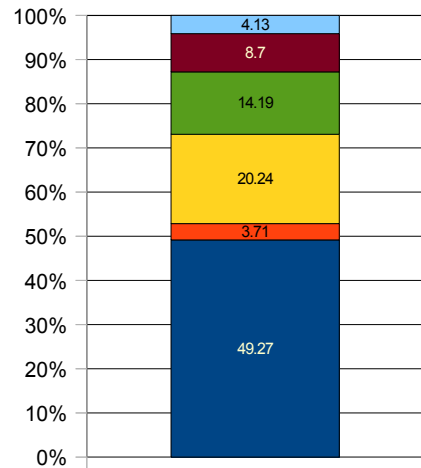


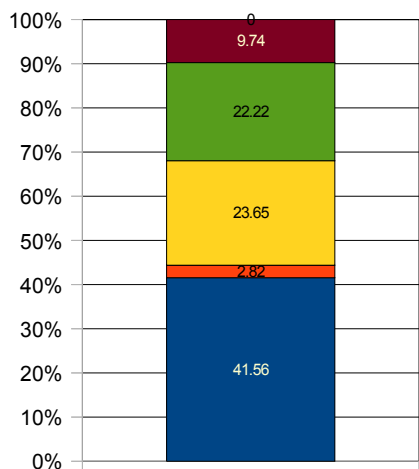
Figure 7: Hub drag, side force and lift coefficients for different configurations normalized by the values of TC1.a



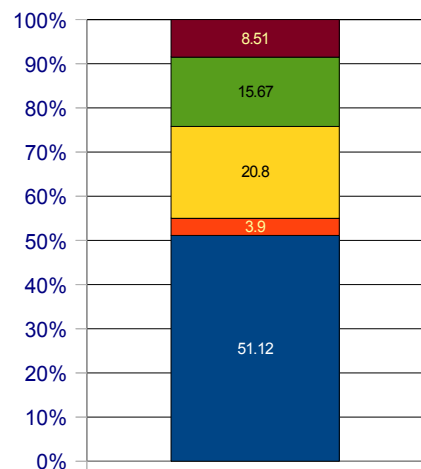
TC1.a



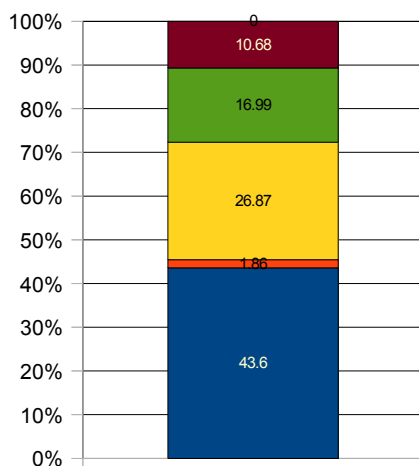
TC1.b



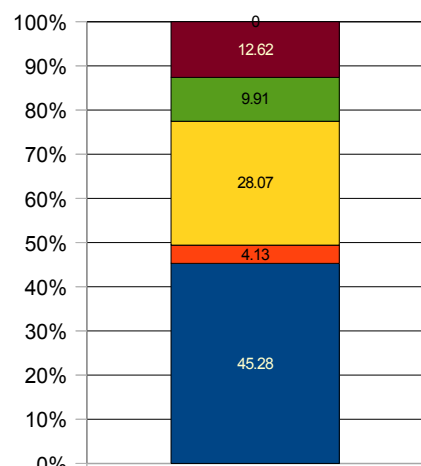
TC2.a



TC2.b



TC3



TC4

Figure 8: Hub drag breakdown

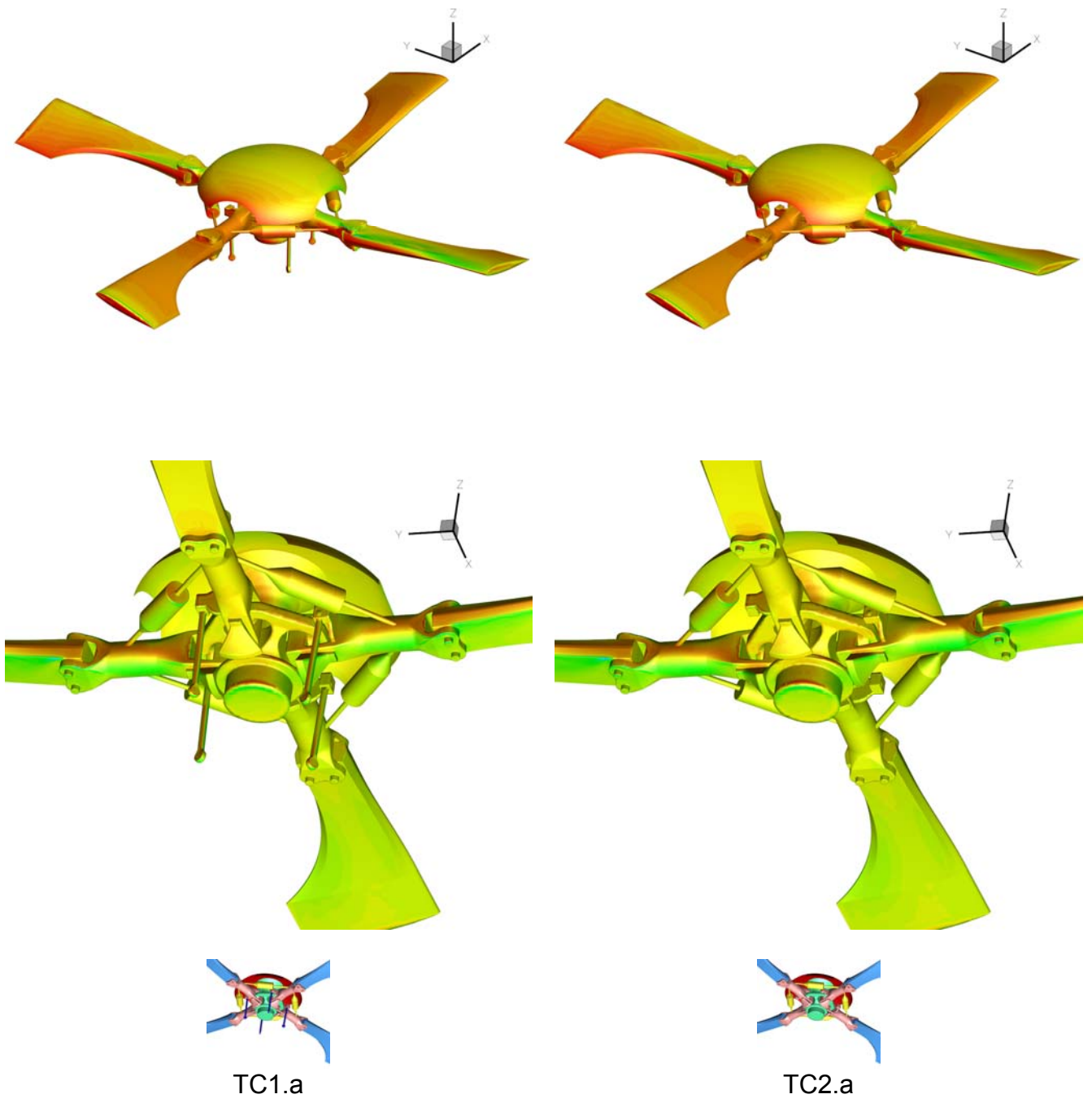


Figure 9: Pressure contours on isolated hub case at  $\alpha=0^\circ$ . Left: full hub. Right: Hub W/O push rods. Top row: upper side. Bottom row: lower side

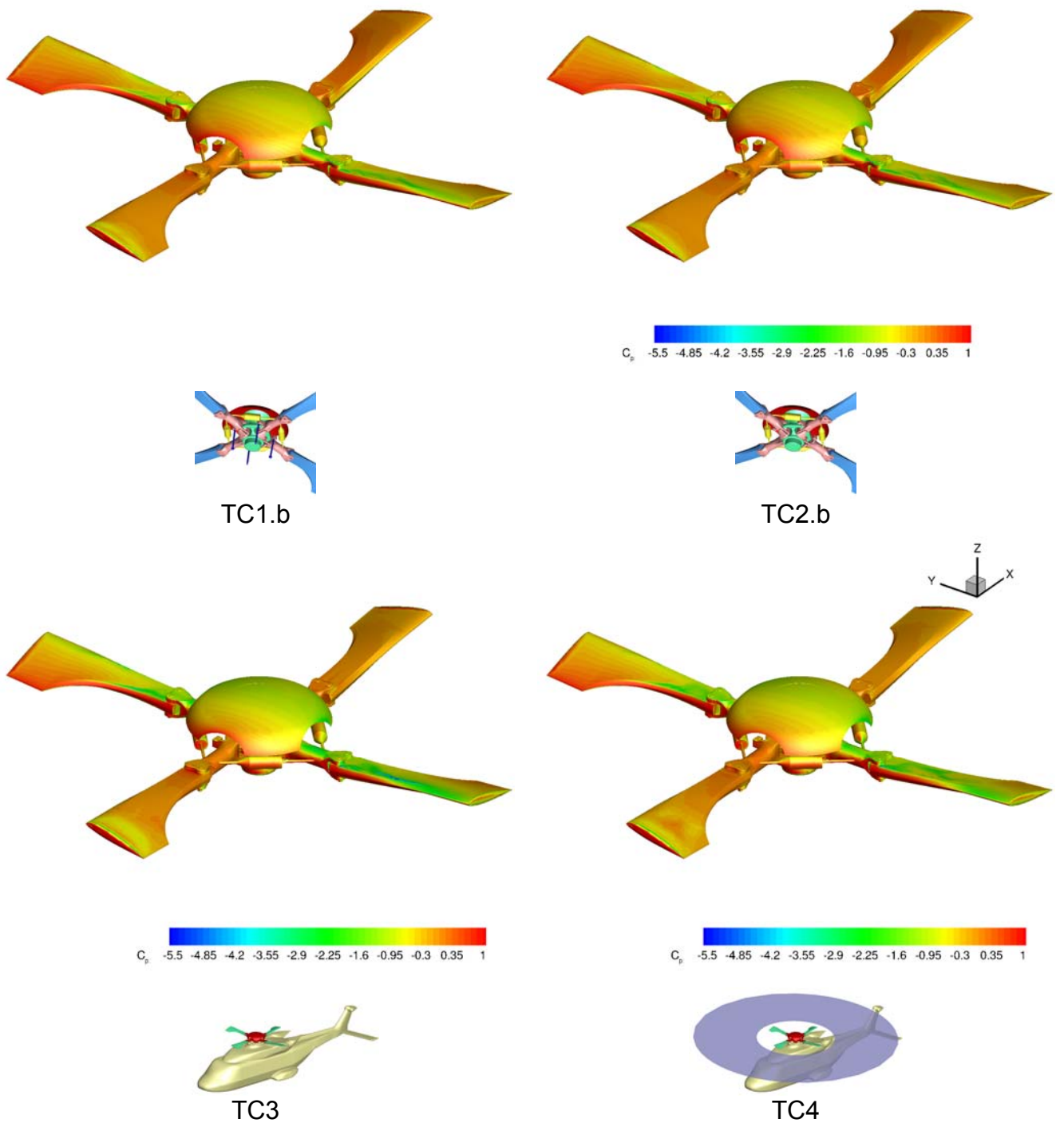


Figure 10: Pressure contours on the hub upper surface  $\alpha = -5^\circ$ .

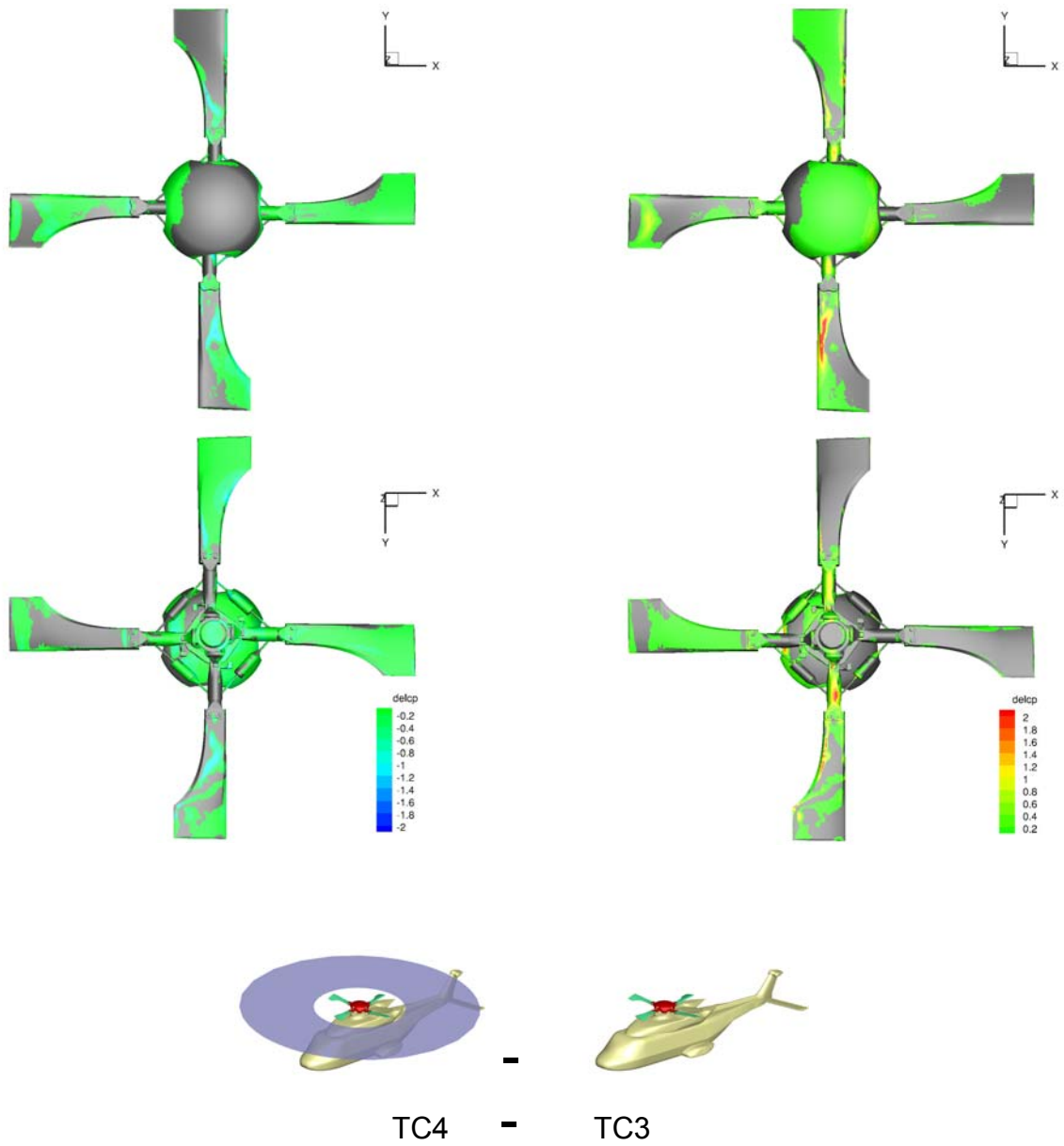


Figure 11: Effect of actuator disc on the rotor hub in terms of  $\Delta C_p$  (TC4-TC3). Left: suction zones. Right: pressure zones.

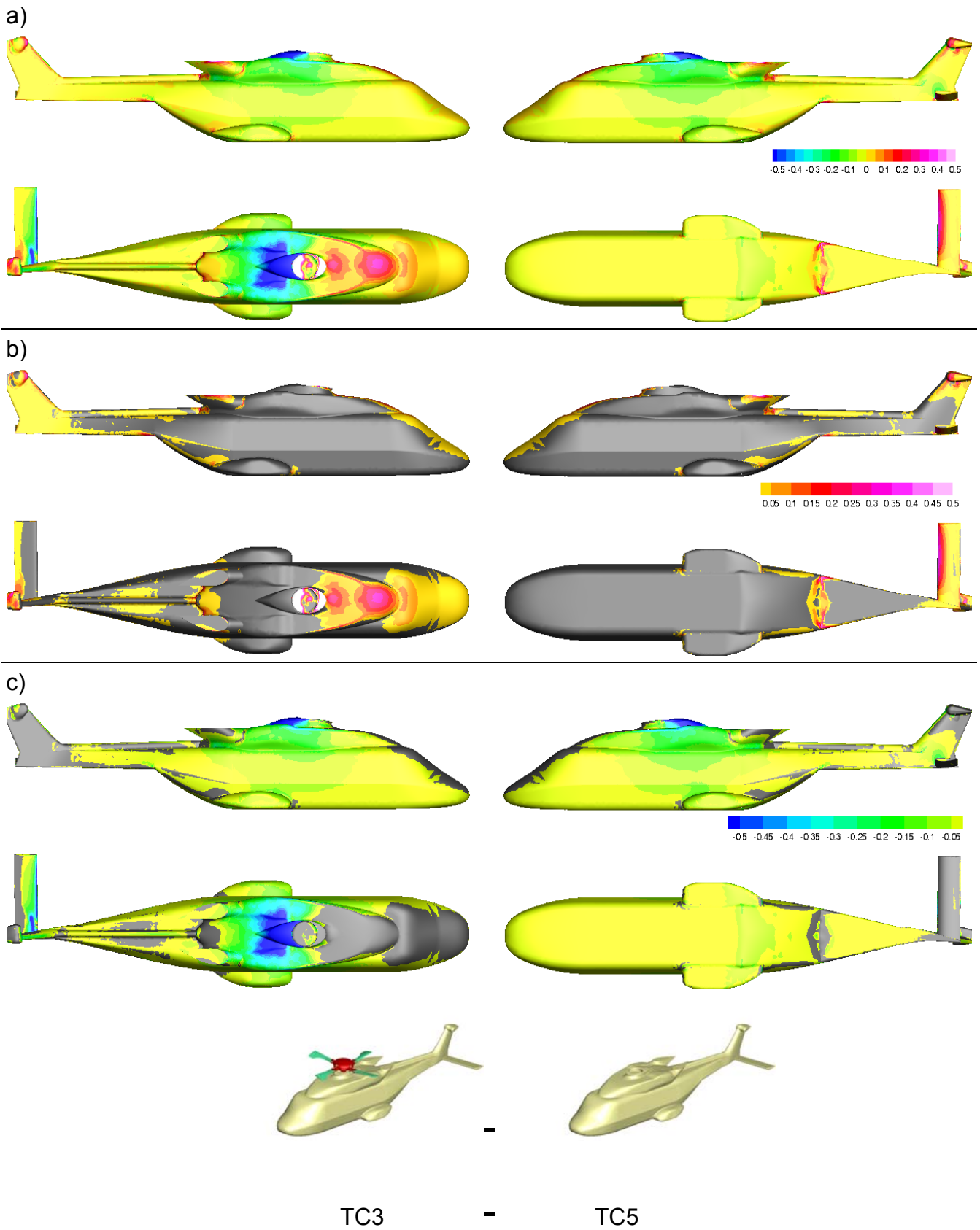


Figure 12: Fuselage surface pressure variation due to the hub. a): Distribution of  $\Delta C_p$  (TC3-TC5) contours on the fuselage. b): Pressure rise zones shown (negative values blanked). c): Pressure drop zones shown (positive values blanked)

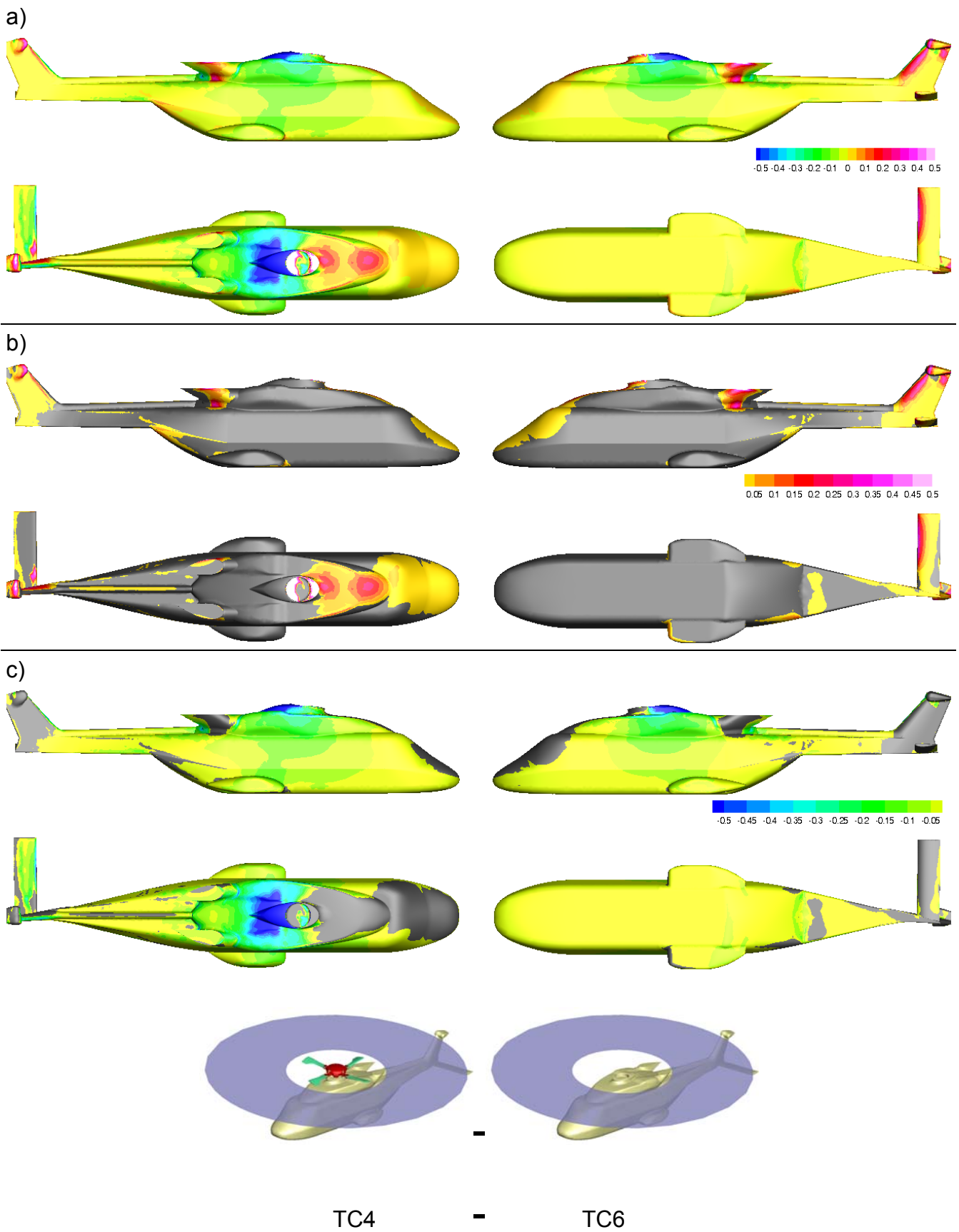


Figure 13: Fuselage surface pressure variation due to the hub. a): Distribution of  $\Delta C_p$  (TC4-TC6) contours on the fuselage. b): Pressure rise zones shown (negative values blanked). c): Pressure drop zones shown (positive values blanked)

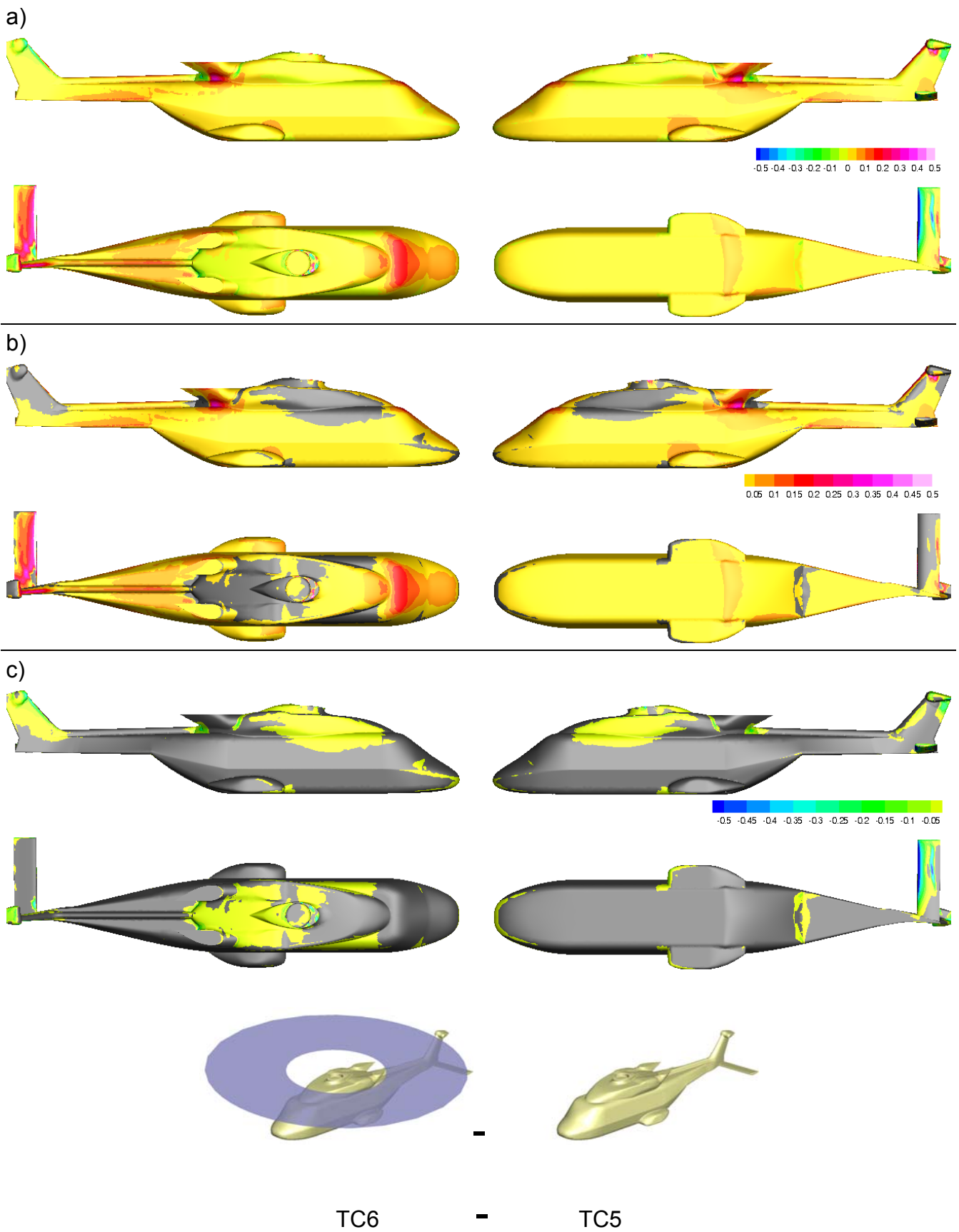


Figure 14: Fuselage surface pressure variation due to the hub. a): Distribution of  $\Delta C_p$  (TC6-TC5) contours on the fuselage. b): Pressure rise zones shown (negative values blanked). c): Pressure drop zones shown (positive values blanked)

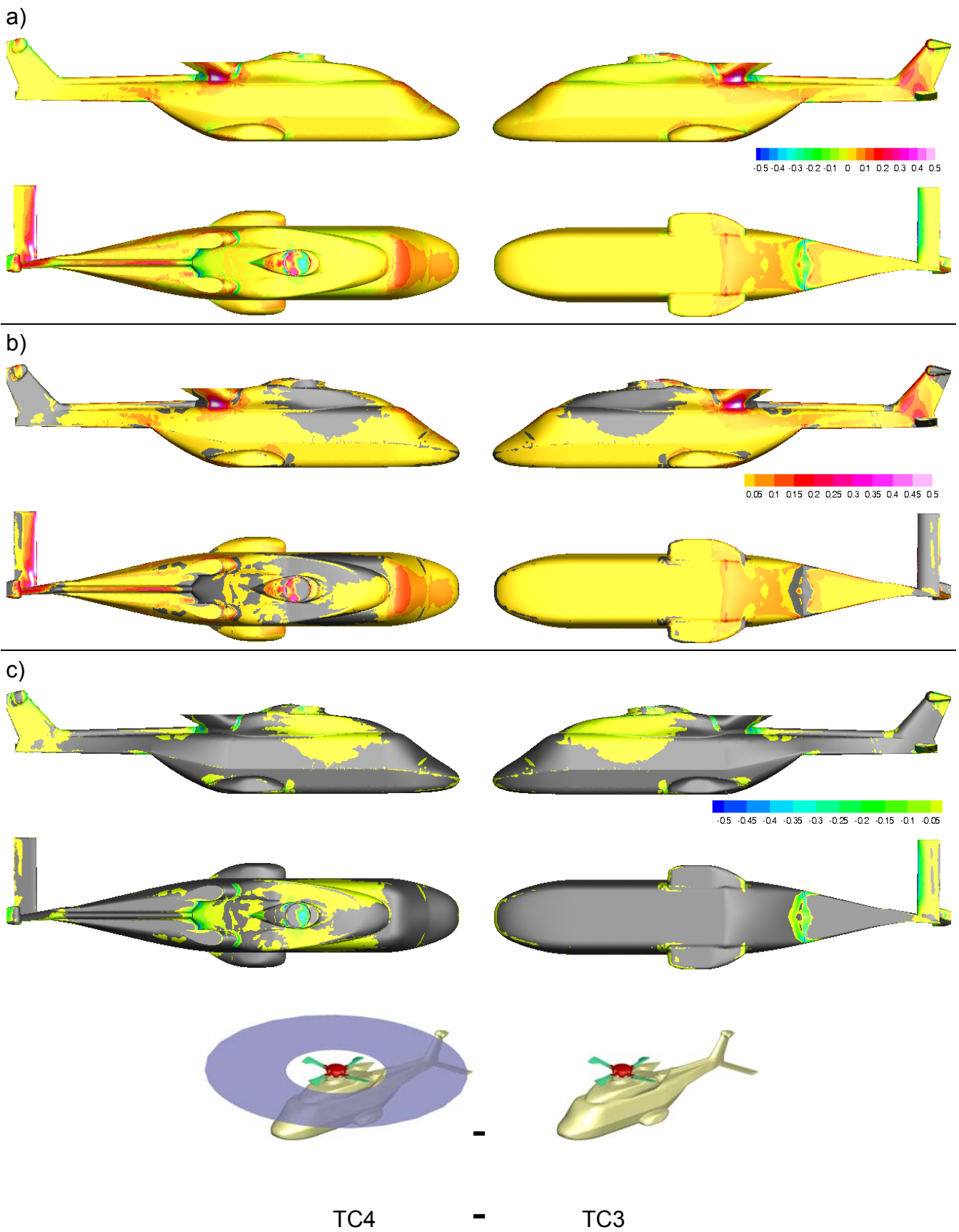


Figure 15: Fuselage surface pressure variation due to the hub. a): Distribution of  $\Delta C_p$  (TC4-TC3) contours on the fuselage. b): Pressure rise zones shown (negative values blanked). c): Pressure drop zones shown (positive values blanked)

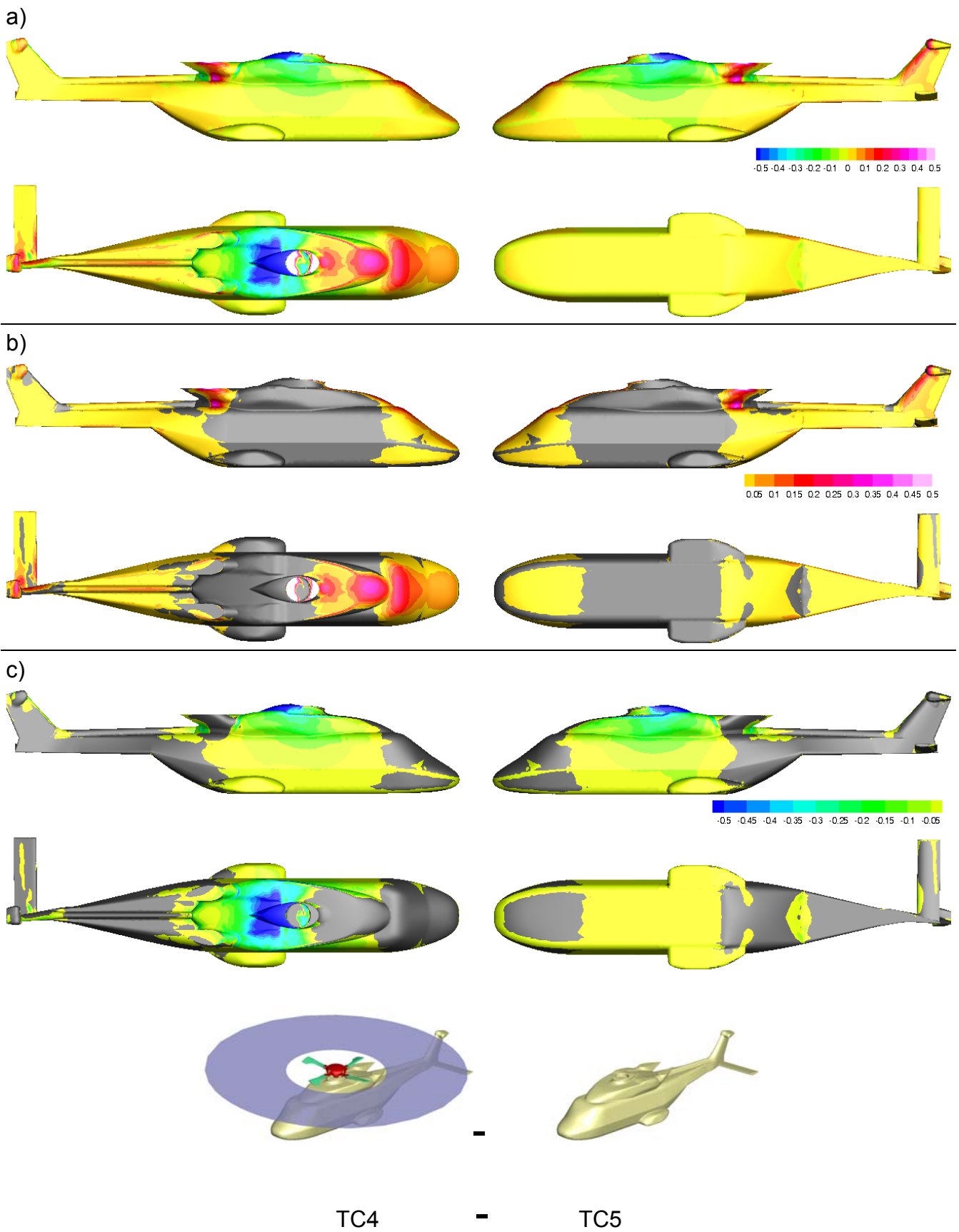


Figure 16: Fuselage surface pressure variation due to the hub. a): Distribution of  $\Delta C_p$  (TC4-TC5) contours on the fuselage. b): Pressure rise zones shown (negative values blanked). c): Pressure drop zones shown (positive values blanked)